SL-2006-166



# Iodination of Gas-Phase-Generated Ag Nanoparticles: Behavior of the Two Spin Orbit Components of the AgI Exciton in Ag@AgI Core−Shell Nanoparticles

**David B. Pedersen* and Shiliang Wang**

*Defence R&D Canada−Suffield, Suffield, Alberta, T1A 8K6 Canada*

*Received: September 27, 2006; In Final Form: October 25, 2006*

Ag nanoparticles, with diameters estimated to be 17 ± 6 nm, were observed to react readily with $I_2$ to produce Ag@AgI core−shell nanoparticles. Both spin−orbit components of the exciton associated with the AgI shell were observed in the UV−vis spectra. The band gap of the AgI shell was found to shift to lower energy as the reaction with $I_2$ proceeded and the shell thickness increased. Shell thickness can be varied by controlling the duration of the exposure of the Ag nanoparticles to iodine. The band gap observed for the Ag@AgI nanoparticles was comparable to that expected of a solid AgI nanoparticle with a diameter of 5−6 nm, as estimated using the Brus formula. The difference between this effective diameter and the actual diameter of the particle (17 ± 6 nm) may be attributable to confinement effects associated with the finite thickness of the AgI shell and/or effects of the Ag core on the AgI shell. The shorter wavelength exciton appeared to be much more sensitive to surface effects, which are pronounced in nanoparticles, and appeared anywhere from 312 to 355 nm. The longer wavelength exciton behaved differently and does not appear to be affected much by such surface effects and therefore seems to be a much more localized electron−hole pair.

## 1. Introduction

Optical properties of metal−semiconductor core−shell nanoparticles are generally well-behaved and have been modeled using Mie theory and similar physical models. In Au@$SiO_2$ nanoparticles, for example, the surface plasmon resonance (SPR) of the Au nanoparticle is preserved but shifted from that of the naked Au nanoparticle of similar size.[1] The sensitivity of the SPR to changes in refractive index of the medium in which the nanoparticle is situated is well-established,[2] and a shift of the SPR to longer wavelengths due to encapsulation of the metal nanoparticle core in a medium of relatively high refractive index, relative to that around the naked particle originally, is expected and predictable. Mie theory has also proven effective for modeling the effect of core and shell sizes on the SPR position.[3] For thin Au shells on AuS cores, as the core size is increased the SPR position is shifted to longer wavelengths, analogous to situating the Au in a medium of relatively high refractive index (i.e., AuS). For a fixed core size, increasing the Au shell thickness from ~1 to 5 nm shifts the SPR to shorter wavelengths. The shift is toward that of bare gold presumably because the relative effect of the core becomes less as the amount of gold increases. Mie theory is found to be consistent with all of these effects. This finding shows that by treating the core−shell particles as two noninteracting media with bulk-like refractive indices many of the optical properties associated with the SPR of the core−shell particles can be understood.

For the semiconductor component of core−shell particles, exciton formation is an absorption feature inherent in the refractive index of the bulk material. Confinement effects are well understood and shift the exciton energy to higher energy as the nanoparticle size is decerased.[4,5] For AgI, such shifts are clearly seen in the spectra of quasi-free AgI nanoparticles as well as during iodination of ultrathin Ag films.[6,7] Accordingly, physical models such as Mie theory which use the refractive index as input "predict" an exciton absorption feature in the model spectra and can also account for shifts due to confinement effects. The exciton absorption of AgI near 440 nm, for example, appears in the calculated spectrum of Ag@AgI nanoparticles.[8] Unfortunately, no experimental data are available to verify the theoretical results. Experimentally, Au@CdS is perhaps the only published spectrum of core−shell nanoparticles where the exciton absorption is obvious.[9] There is a paucity of data on the impact of core size, shell thickness, or core material on the exciton energetics: data required to test the theory. Related work of Lahtinen et al.[10] reported the spectrum of Ag nanoparticles situated in a AgBr matrix and assigned a feature at 516 nm to the AgBr exciton, which would imply a large red-shift from that of bulk AgBr (475 nm). As quantum confinement shifts the band gap to the blue,[4,5] the observed red shift suggests significant charge donation between the shell and core or some similar chemical effect. Such an effect is beyond the limits of Mie theory. Au−AgI nanoparticle pair structures show an exciton peak at 425 nm, which is the bulk value of AgI, and a shift in Au SPR from that of an isolated Au nanoparticle. When there is contact between the Au and AgI nanoparticles, however, the exciton absorption is severely damped, likely due to intermixing of the Au and AgI materials at the boundary between the two particles.[11] For Au@CdS, above band gap absorption of CdS is obvious in the spectrum, but the onset of the exciton absorption is difficult to determine because of overlap of the exciton band edge absorption with the SPR of the Au nanoparticle core. It is clear, however, that, with increasing core:shell molar ratio, increased quenching of the CdS exciton is observed, likely due to an increase in the extent of charge transfer from the CdS to the Au.[9] In contrast to the SPR results described above, these examples of exciton behavior indicate that the core and shell do not behave independently. They interact, and these interactions impact the exciton energetics and dynamics. Accordingly, the pure physical models, such

* To whom correspondence should be addressed. E-mail: david.pedersen@drdc-rddc.gc.ca.

10.1021/jp066357s CCC: $37.00 Published 2007 by the American Chemical Society
Published on Web 12/08/2006

as Mie theory, that appear to describe the SPR behavior may well be inaccurate for the exciton due to its apparent sensitivity to chemical effects.

Recently, we have begun to explore the utility of gas-phase synthesis[12,13] of nanoparticles as an alternative to the more typical solution-phase methods. Potential advantages of the gas phase approach include narrow nanoparticle size distribution, chemically inert synthesis environment (such as vacuum), nanoparticles are pure and naked with no need to functionalize the nanoparticle surface with stabilizers or surfactants as are required to stabilize nanoparticle suspensions, and an ability to synthesize nanoparticles of almost any metal with only minor adjustment of the source conditions. The greatest advantage of the gas phase approach is that it is compatible with quadrupole mass filters that can be used to select particles of specific mass and to narrow the nanoparticle size distribution to unprecedented values. Truly size-dependent properties of the nanoparticles can then be identified and the actual active component of a typically broad size distribution identified. Core−shell nanoparticles[1,14−18] can be made by subsequent exposure of the particles generated in the gas phase source to a reactive gas. Co nanoparticles, for example, naturally oxidize in air to form Co@CoO particles.[19] Similarly, Fe@$FeO_n$ ($n$ = 2 or 3) nanoparticles have been synthesized via controlled surface oxidation of Fe nanoparticles.[20] In this work, we generate Ag@AgI core−shell nanoparticles via exposure of Ag nanoparticles to controlled pressures of $I_2$ vapor. The Ag nanoparticles were synthesized in the gas phase under vacuum. Subsequent exposure to $I_2$ resulted in growth of AgI shells on the order of nanometers thick. This result is compatible with previous work where ambient iodination of Ag films was found to yield nanodimensioned AgI.[21] The Ag nanoparticles and the Ag@AgI particles were characterized through their absorption spectra at ultraviolet and visible wavelengths. Both spin−orbit components of the AgI exciton were observed in the spectra. These spectral features were found to vary in position and intensity as a function of the extent of $I_2$ exposure, extent of particle aggregation, and other factors. Interestingly, the two spin−orbit components of the exciton behave differently and independent of each other. These findings suggest that the extent to which the interaction with the nanoparticle surface occurs is different for the two spin−orbit components of the exciton.

## 2. Experimental Section

Ag nanoparticles were generated in the gas-phase using an aggregation-type source (Mantis Nanogen). A schematic of the apparatus is shown in Figure 1. Briefly, voltage (200−400 V, 200−300 mA) applied between an anode cap and a metal target, in the presence of a few milliTorr of Ar, sustained a plasma inside the region capped by the anode. Ar was introduced at a rate of 10−50 sccm (MKS 1179A mass flow controller) through a shower-head inlet directed at the anode cap and positioned immediately in front of the anode cap. The Ar gas flow could be augmented with a 0−20 sccm flow (MKS 1179A mass flow controller) of He which could be introduced into the aggregation zone through a second gas inlet. Varying the flow of He and Ar allowed the size of nanoparticles generated by the source to be varied. Condensation of the plasma gas began once the plasma gas exited the plasma region, through a hole in the anode cap and entered the first aggregation zone. The gas then expanded into the second aggregation zone, which was evacuated by a 500 L $s^{-1}$ turbo pump (Varian V-550). The nanoparticles thus generated passed through an orifice into the sample chamber where a pressure of $<10^{-4}$ Torr was maintained

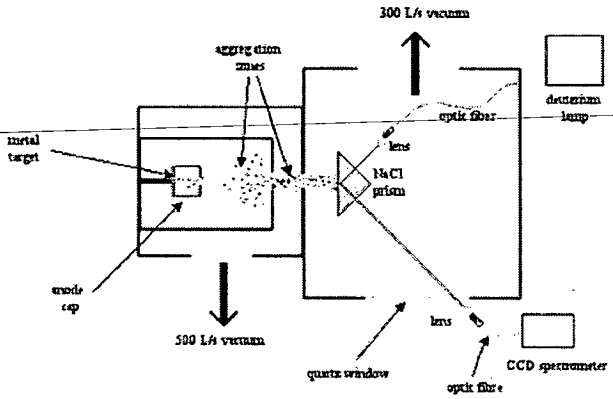


**Figure 1.** Schematic of the apparatus used to generate gas-phase Ag nanoparticles and deposit them onto NaCl substrates. The spectrometer allows the deposition process to be monitored in real time. See text for details.

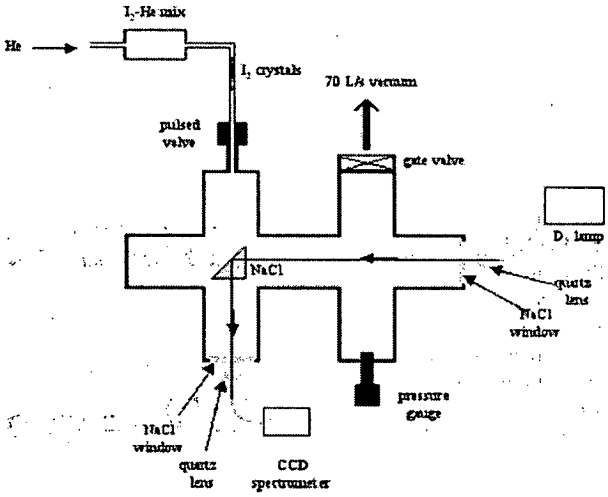


**Figure 2.** Schematic of the gas cell used to do reactivity studies on nanoparticle-coated substrates. See text for details.

during deposition by a 300 L $s^{-1}$ turbo pump (Varian TV-301). The nanoparticles were deposited onto a NaCl prism (International Crystal Laboratories) positioned in the nanoparticle beam path. Light from a deuterium lamp (Mikropak DH-2000) was directed into the sample chamber through an optic fiber, passed through a collimating lens, through one side of the prism, was reflected, and left the sample chamber through a quartz window as shown in Figure 1. The reflected light was then collected by a second collimating lens and focused into another optic fiber which carried the light to the CCD array spectrometer (Ocean Optics-SD2000). The spectrometer was set to acquire spectra every 2−3 s during deposition so that spectra of the nanoparticles could be acquired in real time, as they were being deposited. Deposition times varied from 30 s to 8 min for different samples.

The Ag nanoparticle-coated prisms were removed from the sample chamber of the deposition apparatus and placed in the gas cell depicted schematically in Figure 2. Spectra of the nanoparticle film were collected in real time using a system of collimating lenses and optic fibers, analogous to those used in the deposition apparatus, as shown in Figure 2. An $I_2$−He gas mix was introduced through a pulsed valve (900 series solenoid valve, 0.03″ orifice, powered by an Iota One driver, Parker-Hannifen) directed at the nanoparticle-coated face of the NaCl prism. He gas passed through a 150 mL reservoir in-line with

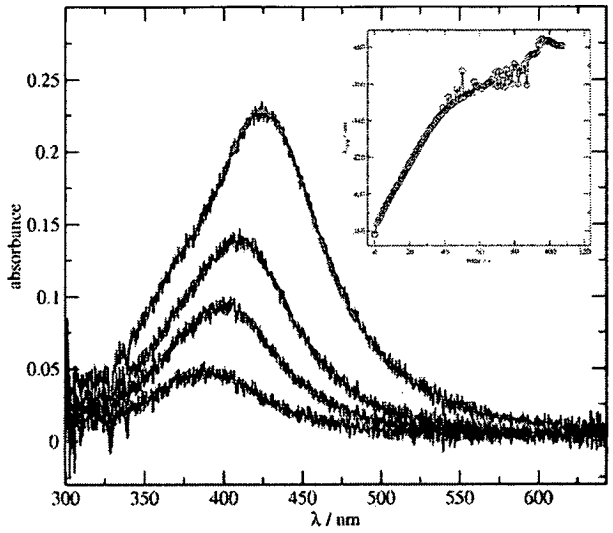


**Figure 3.** Absorbance (extinction) spectra of Ag nanoparticles deposited onto a NaCl substrate. From bottom to top the different spectra correspond to increasing deposition time. $\lambda$ denotes wavelength. The broken red line is a sample fit of the Pearson equation to one of the spectra (see text for details). The inset shows the position of the peak of maximum absorbance ($\lambda_{SPR}$) of the surface plasmon resonance band of Ag nanoparticles as a function of deposition time.

a 1/4″ diameter tube packed with $I_2$ crystals. $I_2$ sublimation saturated the vapor in the reservoir. To help ensure saturation, the gas mix was passed through the $I_2$-packed tube before reaching the pulsed valve. A backing pressure of 7 psi was maintained on the valve. During reaction, the pulsed valve was operated at 2−10 Hz, for the different runs. The pulse duration was 0.5 ms. The gas cell was evacuated by a 70 L $s^{-1}$ turbo pump (Varian V-70). This combination of pumping speed and valve settings resulted in a flow-type condition where the pressure in the cell remained effectively static. The repetition rate of the valve had to be lowered to 0.1 Hz before the cell pressure was seen to rise when the valve fired and subsequently decrease as the cell was evacuated. By varying the rep. rate of the pulsed valve and by partially closing the gate valve, the static pressure in the cell could be varied from a few milliTorr to ~500 Torr. In a typical run, the spectrometer was set to acquire spectra every 2−3 s, and the pulsed valve was then started so that a fixed pressure of $I_2$-He gas mix was maintained in the cell. The spectra were seen to change upon exposure to the reactant gas mix. The run was stopped once changes in the spectra were no longer observable (i.e., the reaction was over).

## 3. Results

In situ monitoring of the deposition of Ag nanoparticles, generated in the sputtering-aggregation source, onto NaCl prism substrates yielded UV−vis spectra like those shown in Figure 3. The spectra have a broad, intense absorption near 380 nm corresponding to excitation of the surface plasmon resonance (SPR) of Ag nanoparticles. With increasing deposition time, the spectra shifted smoothly to longer wavelengths. The shift is co-incident with the decreased average interparticle separation of the nanoparticles that is expected to occur as the number of particles on the NaCl substrate increases with deposition time. In previous work, we have shown that a Pearson function of the form

$$a + \frac{b}{\left(1 + 4\left(\left(\frac{\lambda - c}{d}\right)^2 2^{(1/e)-1}\right)\right)^e} \quad (1)$$

provides a good fit of the SPR absorption[22] as illustrated by the sample fit shown in Figure 3. *a*, *b*, *c*, *d*, and *e* are parameters that are varied to attain the best fit, by least-squares method, to the SPR band. Once a fit is obtained, *c* corresponds to the peak position of maximum absorbance. Fitting all of the spectra acquired during the deposition of the Ag nanoparticles on the salt allows the SPR peak position to be plotted as a function of deposition time, as shown in the inset of Figure 3. The SPR peak position is seen to shift nearly linearly to longer wavelengths until about 40 s, and then there is distinct curvature. We have no evidence as to why the trend changes from linear to curved near 40 s, but such a result is compatible with the average interparticle spacing decreasing to the point where all nanoparticles are somewhat coupled at 40 s (i.e., there are no more isolated nanoparticles on the surface). After this time, further deposition enhances coupling by decreasing the interparticle spacing further. Alternatively, the plateauing could be indicative of formation of nanoparticle aggregates which, at 40 s, have become large enough that increasing their size further causes no noticeable change in SPR position.[23]

The UV−vis spectra of nanoparticle samples exposed to ~$10^{-9}$ Torr of $I_2$ in the gas cell were seen to change significantly in time. After some minutes of exposure, the reaction was over and the spectra remained static. Some of the spectra acquired once the reaction was complete are shown in Figure 4. The spectra are difference spectra; the spectrum of the nanoparticle sample before exposure to $I_2$ has been subtracted from each one. Spectra are dominated by loss of the SPR, near 450−500 nm, associated with the Ag nanoparticles. In addition to the SPR, features associated with AgI are also observed in the spectra. These are observed near 310 and 430 nm and correspond to the two spin orbit components of exciton excitation in AgI.[24,25] The observation of these features is indicative of conversion of Ag to AgI upon exposure of the Ag nanoparticles to the $I_2$ vapor. With uptake of iodine, the SPR of the Ag nanoparticles, which is sensitive to changes in the refractive index of the medium at or near the particle surface, shifts steadily to longer wavelengths as seen in the inset shown in Figure 4. As for Figure 3, the SPR peak position in the inset of Figure 4 was determined by fitting the Pearson expression, eq 1, to the SPR absorbance bands of a series of spectra of the Ag nanoparticles collected in situ and in real time as the nanoparticles were exposed to $I_2$ vapor in the gas cell.

Variability in the peak positions of the absorptions (~310 and 430 nm) associated with two spin orbit components of the AgI exciton was also observed. The 430 nm feature was observed to shift to longer wavelengths as the conversion of the nanoparticles to AgI proceeded. In light of the knee-like shape of this absorption feature (as seen in Figure 4) objective determination of the actual position of this peak directly could be difficult and so was determined by looking at the first derivative of the absorption spectrum. Sample derivative spectra are shown in the inset of Figure 5. As seen, the derivative spectrum is dominated by a feature near 430 nm that corresponds to the "knee" feature of the AgI spectrum. Using the dotted line in the inset of Figure 5 as a reference, a distinct shift of the peak position to shorter wavelengths as one goes from the bottom to the top spectrum is observable. By fitting Gaussian functions to the peaks in the derivative spectra, the position of the ~430 nm band was determined for a series of spectra collected in real time as the Ag nanoparticle samples were

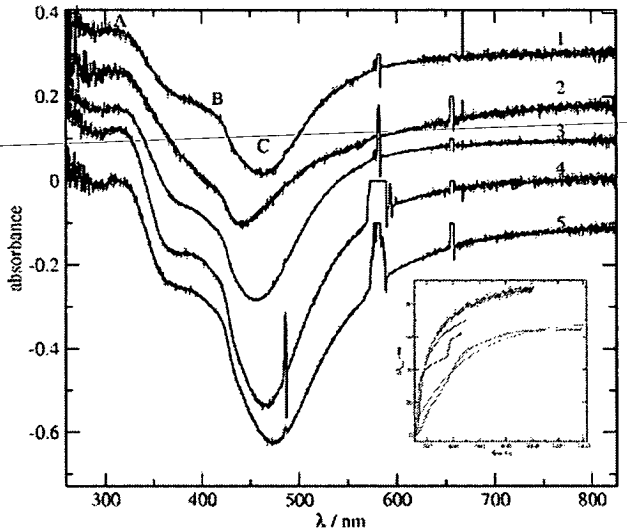


**Figure 4.** Difference spectra of the change in absorption (extinction) that occurred after exposure of five different Ag nanoparticle samples, deposited on NaCl, to ~$10^{-9}$ Torr of $I_2$ vapor for a period of minutes. Features labeled A and B are absorptions characteristic of AgI, absolute spectra of which are shown in Figure 6. C is the surface plasmon resonance of the Ag. The irregular 'spikes' in the spectra near 490, 590, and 660 nm are artifacts caused by room light being reflected into the optic fiber used to input light into the UV−vis spectrometer. $\lambda$ denotes wavelength. In the inset, the change in the position of the peak of maximum absorbance of the surface plasmon resonance band ($\Delta\lambda_{max}$) of Ag nanoparticles is plotted as a function of time of exposure to $I_2$. The pressure of $I_2$ was in the order of $10^{-9}$ Torr for all five runs. The nanoparticles were situated on a NaCl substrate.

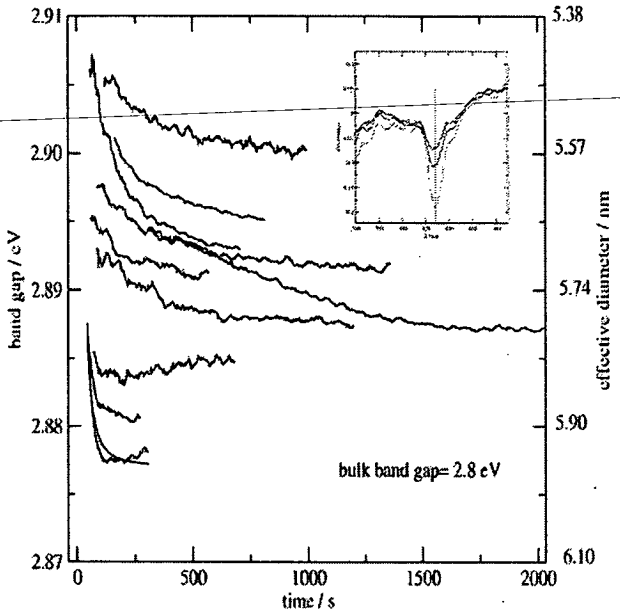


**Figure 5.** Position of the peak in the derivative spectra (band gap), like that shown in the inset, as a function of time of exposure of Ag nanoparticles to $I_2$ vapor. The $I_2$ partial pressure was about $10^{-9}$ Torr. The different traces correspond to different nanoparticle samples. The effective diameter (right $y$ axis) was calculated from the left $y$-axis values using the Brus formula (see text for details). Note that this makes the right $y$ axis nonlinear. The inset shows first derivative of absorption (extinction) spectra of a sample of Ag nanoparticles, on a NaCl substrate, in the region near the onset of exciton absorption (labeled B in Figure 4). The three derivative spectra shown were taken after different exposure times to $I_2$: the uppermost spectrum at the shortest time and the lowermost at the longest time. The dotted line marks the peak position for the bottom spectrum. The derivative spectrum was determined using the finite differences approach. $\lambda$ denotes wavelength.

exposed to $I_2$. A sampling of results is shown in Figure 5, and a shifting of the band to longer wavelengths (lower energy) as the reaction with $I_2$ proceeds is obvious. As this feature of the absorption spectrum of AgI corresponds to the onset of the above band gap excitation, the peak positions have been converted to units of eV to facilitate comparison with literature. Spectra of the shorter wavelength spin orbit component of the AgI exciton near 310 nm are shown in Figure 6 where the position of the short wavelength spin−orbit component of the AgI exciton is marked with dashed lines. As seen, the position of this band was significantly different for different nanoparticle samples and shifts much greater than those observed for the long wavelength component (band near 430 nm) occurred. The type of variability in peak position of the short wavelength exciton band is illustrated in the inset of Figure 6 where the band position is plotted as a function of the SPR peak position of the Ag nanoparticle sample before exposure to $I_2$. No obvious correlation exists between exciton position and SPR peak position. Relatively large variation of the exciton peak position, however, is obvious.

## 4. Discussion

**4.1. Formation of Ag@AgI.** The Ag nanoparticles deposited from the plasma source onto NaCl substrates have absorption spectra characteristic of relatively small nanoparticles. As seen in Figure 3, spectra have a dominant absorption between 400 and 500 nm corresponding to excitation of the surface plasmon resonance of the Ag nanoparticles. The band shifts to longer wavelengths with increased deposition time, as shown in Figure 3, consistent with increased coupling between the Ag nanoparticles on the NaCl surface. The shift in the SPR peak position reflects the increase in particle density on the surface. As the number of nanoparticles on the surface increases, the average interparticle spacing decreases so that the particles get close enough to each other that there is coupling between the particles. Such coupling is well-known to shift the surface plasmon resonance to longer wavelengths as observed.[26−28] Ultimately, at long deposition times, the SPR peak position corresponds to that of a Ag nanoparticle encased in a matrix of Ag nanoparticles. In the inset of Figure 3, the shift in SPR peak position is shown as a function of deposition time. At the earliest times, when the signal:noise ratio in the optical spectrum is just sufficient that the SPR band can be seen, the SPR peak position is ~380 nm. This value corresponds to a minimum coupling situation and approximates the value for truly isolated particles. Bonding with the NaCl substrate is expected to be purely dispersive and no chemical effect on the SPR peak position is expected. Comparison of the 380 nm value with the data of van Duyne[29] and the theoretical results of Liebsch[30] indicates that the nanoparticles initially deposited have a diameter of 17 ± 6 nm. Using optical data to size nanoparticles can be problematic for smaller nanoparticles and does depend on substrate effects. Accordingly, the 17 ± 6 nm should be taken as a reasonable estimate of the nanoparticle diameter. The value is consistent with the type of gas-phase aggregation source used, which is designed to deliver nanoparticles between 0 and 20 nm in diameter.

Exposure of Ag to $I_2$ is a well-established process in the making of photographic film[31,32] and is well-known to form AgI. For the reaction

$$Ag_{(s)} + I_2 \rightarrow 2AgI \qquad (2)$$

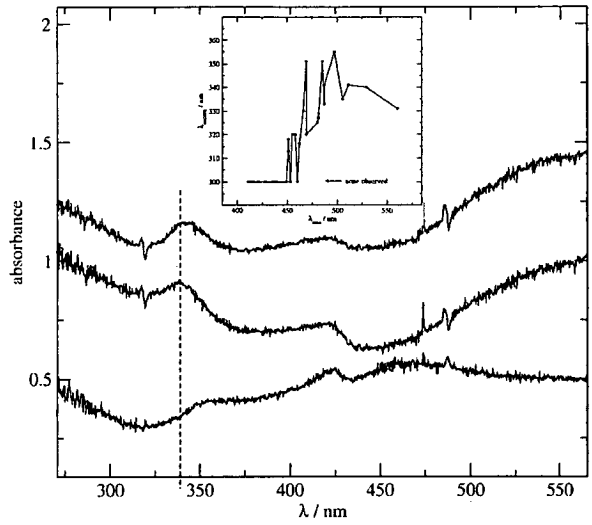


**Figure 6.** Absorption (extinction) spectra of Ag nanoparticle samples after exposure to $I_2$ vapor. The features near 350 and 450 nm correspond to the two spin−orbit components characteristic of AgI. The dotted line marks the peak position of the low wavelength component of the exciton, for the middle spectrum, and is shown to help the eye see that the peak position of this band is different in each spectrum. $\lambda$ denotes wavelength. In the inset, the peak position of maximum absorbance of the short wavelength component of the AgI exciton ($\lambda_{exciton}$) is plotted as a function of the peak position of maximum absorbance of the surface plasmon resonance of the Ag nanoparticles ($\lambda_{max}$) before exposure to $I_2$. Each point corresponds to a different Ag nanoparticle sample. The Ag nanoparticles are situated on a NaCl substrate. Samples where the short wavelength exciton was not observed are given a value of 300 nm, so as to fit on the graph.

the dissociation energy of $I_2$ is 62.42 ± 0.08 kJ mol$^{-1}$, the bond strength of AgI is 291 kJ mol$^{-1}$, and the heat of vaporization of silver is 250.58 kJ mol$^{-1}$.[33,34] The overall reaction is therefore exothermic by 18 kJ mol$^{-1}$. Furthermore, in light of the relatively high electron affinity of $I_2$ (2.5240 ± 0.0050 eV)[35] and the relatively low work function of Ag (4.26 eV for polycrystalline Ag),[36] a harpoon type reaction mechanism is feasible. Charge transfer from the Ag to the $I_2$ becomes exothermic when the Ag−$I_2$ distance is below ~1 nm. Accordingly, one can expect a barrierless reaction path from reactants to products to be present at relatively large distances, and the reaction should occur readily. Experimentally, upon exposure of the Ag nanoparticles to partial pressures of $I_2$ in the $10^{-9}$ Torr range, depletion of the silver SPR was observed within 1 min. This depletion was accompanied by growths near 325 and 425 nm, which are characteristic absorptions of the two spin orbit components of exciton excitation in bulk AgI or AgI nanoparticles.[11,24] The change of spectral features is illustrated in Figure 4. These difference spectra show extensive loss (negative absorbance) of the Ag SPR (labeled C) as well as the growth of the low and high-energy spin orbit components of the AgI exciton (labeled B and A, respectively).

Loss of the surface plasmon band, or more specifically a loss of the low wavelength component and growth at longer wavelengths, occurs whenever the refractive index of the medium surrounding nanoparticles increases and is therefore, by itself, not characteristic of chemical reaction. It can be caused, for example, by physisorption of $I_2$ on the surface of the particles. The appearance of absorption features characteristic of AgI, however, does confirm that a chemical reaction is occurring. Accordingly, monitoring the SPR position as a function of reaction time gives some indication of the extent of conversion of the Ag nanoparticles to AgI. Sample data are shown in the inset of Figure 4 where the position of the SPR band of the Ag is shown as a function of the time that the nanoparticles are exposed to $I_2$ vapor. The SPR shifts smoothly to longer wavelengths as the nanoparticles are converted from Ag to AgI, which is most consistent with an AgI shell or islands of AgI forming on the Ag nanoparticle surfaces. Due to the relatively small size of these particles (17 ± 6 nm), shrinkage of the Ag core due to conversion to AgI is not expected to shift the SPR (to lower wavelengths) significantly. The SPR peak position is relatively size independent for nanoparticles with diameters less than ~25 nm.[37−41] Formation of a hollow Ag core, due to the Kirkendall effect,[42] or change of the Ag core to a more oblate shape are possibilities that we cannot rule out. However, the SPR and exciton behaviors are consistent with the more simpler interpretation of core−shell formation. This is certainly the case in solution where reaction of Ag nanoparticles with iodine yields Ag@AgI structures in which the core is stable and the overall shape of the nanoparticle does not change significantly.[43] During reaction of the NaCl-deposited Ag nanoparticles with $I_2$, the AgI formed cannot be leaving the Ag nanoparticle surface as such a reaction mechanism would not manifest a shift of the SPR to longer wavelengths. Similarly, the appearance of the exciton absorption of AgI in the spectra as the reaction proceeds is evidence of formation of relatively large pieces of AgI; large enough to have a band gap (exciton) near 430 nm. Typically quantum dots lose their band structure when their effective diameters decrease below ~1 nm.[44] The band gaps observed for AgI (Figure 5) lie in the 2.875−2.910 eV range which is comparable to the band gap of a AgI nanoparticle with a diameter of 5.4−6.0 nm (see below). Clearly the spatial dimensions of the AgI formed must be at least comparable to 5−6 nm, which is most compatible with formation of an AgI shell about the Ag core rather than little islands of AgI. In this context, these results are most compatible with Ag@AgI core−shell formation. The magnitude of the SPR shifts, as much as 90 nm as seen in the inset of Figure 4, are consistent with encapsulation of Ag nanoparticles in an AgI matrix. Mie theory predicts the SPR of a 3 nm Ag particle encapsulated in a relatively thin 0.75 nm AgI shell is shifted almost 40 nm from the SPR of the noncapsulated Ag particle.[8] Shells slightly thicker are consistent with the 90 nm shift observed. In combination, all of these findings indicate that the reaction of Ag nanoparticles with $I_2$ results in AgI shell formation about a Ag core. In this context, the shift of the SPR in Figure 4 and the shift of the AgI band gap (Figure 5) in time reflects the effect of increasing AgI shell thickness as the reaction proceeds. This conclusion is also compatible with the work of the Foss group who found the AgI exciton absorption was quenched upon contact of AgI with Au nanoparticles due to intermixing of the AgI and Au phases.[11] Accordingly, the fact that the AgI exciton is observed in our spectra indicates an absence of intermixing of the AgI and Ag phases, which is most consistent with a core−shell structure.

**4.2. Exciton Behavior.** With exposure to $I_2$, the conversion of the surface of Ag nanoparticles to AgI manifests growth of an AgI shell from an initial thickness of near zero to a thickness of at most ~10 nm (which would constitute 100% conversion of the silver to silver iodide). In this regime, confinement effects are well-known to impact the energetics of exciton excitation in band gap materials.[4,5] For the AgI shell, the onset of exciton absorption appears as a knee in the spectra observed, feature B in Figure 4. This feature is accentuated by taking the first derivative of the absorbance, some examples of which are shown in the inset of Figure 5. By fitting Gaussian functions to the

peak in the derivative spectrum, the peak position was determined for a series of spectra, and results are shown in Figure 5 for a number of Ag nanoparticle samples as a function of time of exposure to $I_2$. Differences between the various traces are thought to reflect variability in the Ag nanoparticle sizes and extent of aggregate formation due to slightly different source and deposition conditions as well as to differences in the roughness of the NaCl substrates on which the nanoparticles were deposited. Despite these differences, the overall shapes of the traces are similar. Initially, they exponentially decrease to lower energy with increased exposure time; at longer exposure times they asymptotically approach a constant value. Bulk AgI can assume both wurtzite and zinc-blend structures with band gaps of ~2.8 and ~2.4 eV, respectively.[45-47,24] The asymptote approached in Figure 5 is close to the wurtzite value, although there is up to 0.3 eV variability in the asymptote approached for the different samples. The variance could be attributable to differences in the final shell thickness obtained and the overall diameter of the Ag@AgI nanoparticle. It may also reflect difference in the crystalline structure that the AgI shell assumes, which is likely polycrystalline to some extent.

The exponential decrease in energy is the trend expected of a band gap material whose dimensions are systematically being increased, which is consistent with increasing AgI shell thickness as the Ag + $I_2$ reaction proceeds. Semiconductor band gaps experience an analogous exponential-like decrease in band gap as the diameter of the quantum dots is increased. To first order the band gap of a semiconductor nanoparticle is given by the Brus formula

$$E_{nano} = E_{bulk} + \frac{h^2}{2m^*d^2} - \frac{1.8e^2}{2\pi\epsilon\epsilon_0 d} \quad (3)$$

where $E_{nano}$ is the band gap of the nanoparticle, $E_{bulk}$ is the band gap of the bulk semiconductor, $h$ is Planck's constant, $m^*$ is the reduced mass of the exciton, $d$ is the diameter of the nanoparticle, $e$ is the charge on an electron, $\epsilon$ is the dielectric constant of the semiconductor, and $\epsilon_0$ is the vacuum permittivity. For AgI, appropriate values of the material-specific parameters are $m^* = 0.185$ and $\epsilon = 5.6$.[45] Substitution of these values into eq 3 allows the effective diameter ($d$) of the AgI generated in the Ag nanoparticle–$I_2$ reaction to be determined by substituting band gap values, taken from Figure 5, for $E_{nano}$. The results are illustrated in Figure 5 where the right $y$ axis is labeled with the effective diameter calculated for the corresponding value shown on the left $y$ axis (note that this makes the right axis nonlinear). Interestingly, even at early reaction times where the AgI shell thickness is relatively thin, the band gap observed for the Ag@AgI particles corresponds to that of a solid AgI nanoparticle with a diameter of between 5 and 6 nm. That is, the AgI shell behaves as if it had a diameter, its effective diameter, of 5–6 nm. Given that the excitons generated in the AgI shell are free to travel over the entire surface of the nanoparticle, the effective diameter should be close to that of the original Ag nanoparticle (estimated to be 17 ± 6 nm). The difference between the effective diameter and the actual particle diameter may be attributed to confinement (due to the fact that the AgI appears as a shell as opposed to a solid AgI particle) and/or to effects of the Ag core on the AgI shell. There is also some error in the 17 ± 6 estimated particle size that may account for some of the difference. However, in light of the relatively large difference between 5 and 6 nm and 17 ± 6 nm values of the effective and actual particle diameters, it is very likely that confinement within the shell and the influence of the Ag core do play a role in determining the band gap measured. Accordingly, systematically varying these parameters (shell thickness and core material or size) over a larger range should afford an opportunity to tune the band gap of the AgI shell over a relatively large range.

The second spin–orbit component of the AgI exciton appears near 330 nm in the spectra of Ag@AgI nanoparticles (feature A in Figure 4). In contrast to the long wavelength component of the exciton, which was always observed at 429 ± 3 nm, the short wavelength band varied widely in position, from 312 to 355 nm, for the different samples. The difference in behavior of the two bands is illustrated in Figure 6. As seen, the long wavelength component of the exciton absorption occurs near 425 nm for all three samples shown, but the component near 350 nm is seen to vary by more than 10 nm. Similar behavior has been observed when the temperature of single-crystal AgI samples is varied; the long wavelength feature shows little temperature dependence, while the short wavelength component changes significantly.[24] The height of the short wavelength component, relative to the long one, also varies more significantly, at times becoming larger than the long wavelength component. Similar spectra can be found in the literature for nanoscale AgI.[48] In short, the two bands behave differently. The sensitivity of the short wavelength component to changes in environmental conditions, such as temperature, nanoparticle diameter, extent of nanoparticle aggregation, and the nature of the substrate, most likely indicates that the wavefunction associated with the hole generated upon creation of the exciton is poorly shielded from the AgI surface. As the two spin orbit components of the exciton have different symmetries, it is reasonable to assume that the spatial extent of one, and the extent that it interacts with the AgI surface, is greater than the extent that the other interacts with the surface. In the inset of Figure 6, the position of the short wavelength component of the exciton is plotted as a function of the position of the SPR in the unreacted sample. Interestingly, for samples where the SPR position was less than ~450 nm, no exciton could be observed. This is most likely because the nanoparticle density is quite low for these samples and the spectrometer does not have the sensitivity to detect the small amount of AgI produced. SPR positions less than 450 nm are approaching those of the isolated nanoparticle (see above), which indicates minimal coupling and a low nanoparticle density on the surface. Regardless, for the excitons that were observed, there is no real trend in the data suggesting a correlation between exciton peak position and the extent of nanoparticle coupling. The exciton position is seen to vary by over 40 nm for the different samples. Such variability in AgI peak position far exceeds that observed in single-crystal studies. In light of the nanometer dimensions of the AgI shell in the Ag@AgI particles, most of the constituent AgI molecules reside at or near the inner or outer surfaces of the AgI shell. Accordingly, surface effects are greatly accentuated and variability in the exciton peak position much higher than that observed in bulk AgI is not surprising.

## 5. Summary

Ag nanoparticles, with diameters estimated to be 17 ± 6 nm, were observed to react readily with $I_2$ to produce AgI. Above band gap excitation of the AgI component was readily observable in the UV–vis spectra. The band gap of the AgI, as judged by the onset of absorption in the spectra, was found to shift smoothly to longer wavelength as the reaction with $I_2$ proceeded. So too did the SPR band associated with the Ag. These results are most consistent with the formation of Ag@AgI core–shell nanoparticles during the reaction. To our knowledge, these are the first spectra where the band gap of a semiconductor shell

on a metal nanoparticle core has been observed and seen to be tunable by varying shell thickness. Shell thickness can be varied by controlling the duration of the exposure of the Ag nanoparticles to iodine. The band gap observed for the Ag@AgI nanoparticles is comparable to that expected of a solid AgI nanoparticle with a diameter of ~5−6 nm, as estimated using the Brus formula. The difference between this 5−6 nm effective diameter and the estimated diameter of the particle (17 ± 6 nm) may be attributable to confinement effects associated with the finite thickness of the AgI shell and/or effects of the Ag core on the AgI shell. Accordingly, varying these parameters over a larger range than explored in this work should afford an opportunity to vary the band gap of the AgI component over a larger range.

Both spin orbit components of the AgI exciton were evident in the UV−vis spectra. The two components behaved very differently. The longer wavelength component shifted modestly with change in the duration of exposure to $I_2$ but always appeared at 429 ± 3 nm. In contrast, the shorter wavelength exciton appeared anywhere from 312 to 355 nm for the various samples. The much higher range of wavelengths of the latter suggests that the wavefunction associated with this exciton is poorly shielded from the AgI surface. The range of wavelengths at which this exciton appeared is also much broader than that observed in AgI bulk crystals. The fact that for the AgI shell, and for nanoparticles in general, a large fraction of the constituent AgI molecules reside at or near the inner or outer surface of the shell translates into surface interactions more pronounced than in the bulk crystal medium. The enhanced surface interaction expected in the nanoparticles coupled with the broad range of wavelengths at which the exciton is observed strongly support the notion that this exciton is poorly shielded from the nanoparticle surface. The longer wavelength exciton behaves differently and does not appear to be affected much by such surface effects and therefore seems to be a much more localized electron−hole pair.

## References and Notes


(1) Liz-Marzan, L.; Mulvaney, P. *J. Phys. Chem. B* **2003**, *107* (30), 7312−7326.
(2) Jung, L. S.; Campbell, C. T.; Chinowsky, T. M.; Mar, M. N.; Yee, S. S. *Langmuir* **1998**, *14* (19), 5636−5648.
(3) Averitt, R. D.; Sarkar, D.; Halas, N. J. *Phys. Rev. Lett.* **1997**, *78* (22), 4217−4220.
(4) Brus, L. E. *J. Chem. Phys.* **1984**, *80* (9), 4403−4409.
(5) Rossetti, R.; Hull, R.; Gibson, J. M.; Brus, L. E. *J. Chem. Phys.* **1985**, *82* (1), 552−559.
(6) Mochizuki, S.; Umezawa, K. *Phys. Lett. A* **1997**, *228*, 111.
(7) Mohan, D. B.; Sunandana, C. S. *J. Appl. Phys.* **2006**, *100*, 064314.
(8) Mulvaney, P. *Langmuir* **1996**, *12* (3), 788−800.
(9) Kamat, P. V.; Shanghavi, B. *J. Phys. Chem. B.* **1997**, *101* (39), 7675−7679.
(10) Lahtinen, R.; Mertens, S.; East, E.; Kiely, C.; Schiffrin, D. *Langmuir* **2004**, *20* (8), 3289−3296.
(11) El-Kouedi, M.; Foss, C. *J. Phys. Chem. B* **2000**, *104* (17), 4031−4037.
(12) Qiang, Y.; Sabiryanov, R. F.; Jaswal, S. S.; Liu, Y.; Haberland, H.; Sellmyer, D. J. *Phys. Rev. B* **2002**, *66* (6), 064404.
(13) Antony, J.; Qiang, Y.; Baer, D. R.; Wang, C. *J. Nanosci. Nanotechnol.* **2006**, *6*, 568−572.
(14) Liu, C.; Wu, X.; Klemmer, T.; Shukla, N.; Weller, D.; Roy, A.; Tanase, M.; Laughlin, D. *Chem. Matter.* **2005**, *17* (3), 620−625.
(15) Chakraborty, I.; Mitra, D.; Moulik, S. *J. Nanoparticle. Res.* **2005**, *7* (2−3), 227−236.
(16) Mizukoshi, Y.; Fujimoto, T.; Nagata, Y.; Oshima, R.; Maeda, Y. *J. Phys. Chem. B* **2000**, *104* (25), 6028−6032.
(17) Ah, C.; Kim, S.; Jang, D.-J. *J. Phys. Chem. B* **2006**, *110* (11), 5486−5489.
(18) Kim, H.; Achermann, M.; Balet, L.; Hollingsworth, J.; Klimov, V. *J. Am. Chem. Soc.* **2005**, *127* (2), 544−546.
(19) Imperia, P.; Schmitz, D.; Maletta, H.; Sobal, N. S.; Giersig, M. *Phys. Rev. B* **2005**, *72*, 014448.
(20) Signorini, L.; Pasquini, L.; Savini, L.; Carboni, R.; Boscherini, F.; Bonetti, E.; Giglia, A.; Pedio, M.; Mahne, N.; Nannarone, S. *Phys. Rev. B* **2003**, *68*, 195423.
(21) Kumar, P. S.; Ray, S.; Sunandana, C. S. *Mater. Phys. Mech.* **2001**, *4*, 39−41.
(22) Pedersen, D. B.; Duncan, S. *J. Phys. Chem. A* **2004**, *109* (49), 11172−11179.
(23) Wei, Q. H.; Su, K. H.; Durant, S.; Zhang, X. *Nano Lett.* **2004**, *4* (6), 1067−1071.
(24) Tutihashi, S. *Phys. Rev.* **1956**, *105* (3), 882−884.
(25) Cardona, M. *Phys. Rev.* **1963**, *129* (1), 69−78.
(26) Kelly, K. L.; Lazarides, A. A.; Schatz, G. C. *Comput. Sci. Eng.* **2001**, *3* (4), 67−73.
(27) Lazarides, A. A.; Schatz, G. C. *J. Phys. Chem. B* **2000**, *104* (3), 460−467.
(28) Storhoff, J. J.; Lazarides, A. A.; Mucic, R. C.; Mirkin, C. A.; Letsinger, R. L.; Schatz, G. C. *J. Am. Chem. Soc.* **2000**, *122* (19), 4640−4650.
(29) Zhang, X.; Hicks, E. M.; Zhao, J.; Schatz, G. C.; Van Duyne, R. P. *Nano Lett.* **2005**, *5* (7), 1503−1507.
(30) Liebsch, A. *Phys. Rev. B* **1993**, *48* (15), 11317−11328.
(31) Talbot, W. H. F. *The Pencil of Nature*; Longmans: London, 1844.
(32) Talbot, W. H. F. *The Pencil of Nature*; DaCapo Press: 1968.
(33) Cox, J.; Wagman, D.; Medvedev, V. A. *CODATA Key Values forThermodynamics*; Hemisphere Publishing Corp.: New York, 1984.
(34) Brice, B. A. *Phys. Rev.* **1931**, *38*, 658−670.
(35) Zanni, M.; Taylor, T.; Greenblatt, J.; Soep, B.; Neumark, D. *J. Chem. Phys.* **1997**, *107*, 7613.
(36) Lide, D. R., Ed. *CRC Handbook of Chemistry and Physics*, 73 ed.; CRC Press Inc: Boca Raton, FL, 1992.
(37) Jensen, T.; Kelly, L.; Lazarides, A.; Schatz, G. C. *J. Clust. Sci.* **1999**, *10* (2), 295−317.
(38) Murillo, L. E.; Viera, O.; Vicuna, E.; Briano, J. G.; Castro, M.; Ishikawa, Y.; Irizarry, R.; Sola, L. In *Technical Proceedings of the 2002 International Conference on Computational Nanoscience and Nanotechnology, Chpt 16: Material and Nanostructures Science*, 2002.
(39) Link, S.; El-Sayed, M. A. *J. Phys. Chem. B* **1999**, *103*, 4212−4217.
(40) Hodak, J. H.; Henglein, A.; Hartland, G. V. *J. Phys. Chem. B* **2000**, *104*, 9954−9965.
(41) Link, S.; El-Sayed, M. A. *J. Phys. Chem. B* **1999**, *103*, 8410−8426.
(42) Nakajima, H. *JOM* **1999**, *49* (6), 15−19.
(43) Tan, H.; Fan, W. Y. *Chem. Phys. Lett.* **2005**, *406*, 289−293.
(44) Murray, C. B.; Norris, D. J.; Bawedi, M. G. *J. Am. Chem. Soc.* **1993**, *115*, 8706.
(45) Bedikyan, L. D.; Miloslavskii, V. K.; Ageev, L. A. *Opt. Spectrosc. (USSR)* **1980**, *47* (2), 225−226.
(46) Vogel, D.; Kruger, P.; Pollmann, J. *Phys. Rev. B* **1998**, *58* (7), 3865−3869.
(47) Victora, R. H. *Phys. Rev. B* **1997**, *56* (8), 4417−4421.
(48) Kumar, P. S.; Sundandana, C. S. *Nano Lett.* **2002**, *2* (4), 431−434.

#527026
CA628846